
Improving Medical Multi-modal Contrastive Learning with Expert Annotations

Yogesh Kumar

*Department of Computer Science
Aalto University, Finland*

yogesh.kumar@aalto.fi

Pekka Marttinen

*Department of Computer Science
Aalto University, Finland*

pekka.marttinen@aalto.fi

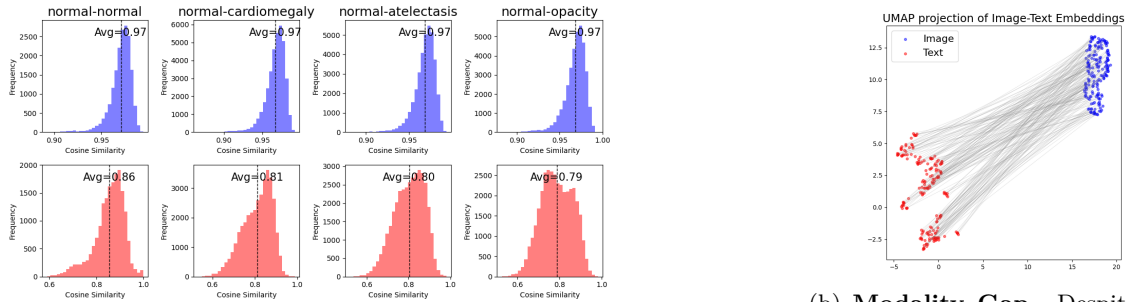
Abstract

We introduce eCLIP, an enhanced version of the CLIP model that integrates expert annotations in the form of radiologist eye-gaze heatmaps. It tackles key challenges in contrastive multi-modal medical imaging analysis, notably data scarcity and the “modality gap” – a significant disparity between image and text embeddings that diminishes the quality of representations and hampers cross-modal interoperability. eCLIP integrates a heatmap processor and leverages mixup augmentation to efficiently utilize the scarce expert annotations, thus boosting the model’s learning effectiveness. eCLIP is designed to be generally applicable to any variant of CLIP without requiring any modifications of the core architecture. Through detailed evaluations across several tasks, including zero-shot inference, linear probing, cross-modal retrieval, and Retrieval Augmented Generation (RAG) of radiology reports using a frozen Large Language Model, eCLIP showcases consistent improvements in embedding quality. The outcomes reveal enhanced alignment and uniformity, affirming eCLIP’s capability to harness high-quality annotations for enriched multi-modal analysis in the medical imaging domain.

1 Introduction

Pretraining foundation models on multi-modal data – particularly leveraging the relationships between text and images – has proven to be a robust strategy for generating versatile embeddings (Radford et al., 2021; Jia et al., 2021). These embeddings enhance the efficacy in several downstream tasks, from image generation to advanced vision-language integration (Liu et al., 2023; Ramesh et al., 2021; Singh et al., 2022). Central to this approach is the employment of a contrastive learning (CL) loss objective (Oord et al., 2018; Chen et al., 2020; Zbontar et al., 2021), where models are trained to align positive pairs (e.g., an image and its corresponding caption) while diversifying negative ones. A significant hurdle in this approach is the necessity of vast datasets, often comprising several millions of data points, for competitive results. Models such as CLIP (Radford et al., 2021) have been trained on internet-scale datasets, estimated to encompass hundreds of millions of image-text pairs (Cherti et al., 2023; Xu et al., 2023a). Acquiring datasets of this magnitude poses substantial challenges in specialized fields that require expert knowledge for data collection, processing and annotation. The medical imaging domain exemplifies these difficulties, where acquiring even a single data point, such as a chest X-ray, involves complex processes requiring expertise and significant resources. Moreover, the procurement of such data for machine learning research is further complicated by ethical considerations, patient privacy concerns and the need for extensive de-identification procedures.

This has led to the prevalent use of foundation models, initialized with weights from models trained on extensive internet-scale datasets, for tasks in the medical domain (Zhang et al., 2022; Wang et al., 2022; Huang et al., 2021; Krishnan et al., 2022). However, the areas of interest within medical images are often nuanced and require expert knowledge to interpret, rendering them indistinguishable to a general-purpose



(a) **Histogram of Cosine Similarities Among Subgroups.** The model exhibits high cosine similarity among embeddings within the text (*red*) and image (*blue*) modalities, regardless of the differences among subgroups. This underscores the model’s challenge in capturing the subtleties inherent in medical data.

(b) **Modality Gap.** Despite the CLIP contrastive loss aiming at closely aligning image and text embeddings within a shared space, the modalities remain segregated into distinct regions.

Figure 1: **Analysis of CLIP Embeddings in Medical Imaging** The figure presents embeddings generated by a CLIP model, pretrained on an internet-scale dataset, applied to the Open-I dataset pairing X-rays with corresponding radiology reports.

model. In 1a, we investigate the embeddings generated by a CLIP model – initially pretrained on internet data – using samples from the Open-I dataset (Demner-Fushman et al., 2016), which includes X-rays and corresponding radiology reports. We categorize the samples into subgroups based on the primary abnormality identified in each report, such as ‘normal’, cardiomegaly, atelectasis and opacity. A histogram of the cosine similarities between embeddings from different groups indicates a high degree of similarity, with values approaching 1. This could lead to potential challenges in downstream zero-shot inference tasks, which rely on the spatial segregation of embeddings from different groups (Radford et al., 2021). Typically, continual pretraining on medically relevant data is employed to enhance the model’s ability to differentiate between various abnormalities.

Recent studies (Liang et al., 2022; Goel et al., 2022; Oh et al., 2023; Zhang et al., 2024; Tschannen et al., 2023) have identified a “modality gap” in multi-modal contrastive representation learning, where the embeddings from different modalities (e.g., images and text) fall in distinct regions in the shared embedding space. This separation, which arises from factors such as initial model weights and the objectives of contrastive learning (Liang et al., 2022; Zhang et al., 2024), leads to the “cone effect” where embeddings of each modality are restricted to a narrow region of the embedding hypersphere. In 1b, we illustrate this within the medical domain with a 2D UMAP (McInnes et al., 2018) projection of image and text embeddings. This example highlights how embeddings from the same modality but different semantic groups, such as X-ray images of varying abnormalities, cluster closely together. This makes it difficult for a model to distinguish between semantically different images, undermining its performance in medical image analysis.

We investigate the potential of integrating expert annotations, specifically radiologist eye-gaze heatmaps, to alleviate these issues. Processing the eye-gaze data from radiologists (Karagyris et al., 2021) provides us with heatmaps indicative of the radiologist’s attention across different regions of the X-ray images. This heatmap reflects areas of clinical interest aligned with details present in radiology reports. We posit that this could help capture nuanced visual cues in the X-rays and therefore pairing it with reports can enrich the CLIP training data with high-quality positive pairs. Due to the scarcity of such expert annotated data, we employ the mixup strategy, a data augmentation technique which has been effective in both supervised (Zhang et al., 2017; Verma et al., 2019; Han et al., 2022) and contrastive learning (Verma et al., 2021; Oh et al., 2023), to create additional synthetic samples.

We present eCLIP (expert-annotated CLIP), an adaptation of the CLIP model that incorporates expert eye-gaze heatmaps, without modifying the CLIP model’s core architecture. The operational workflow of eCLIP is depicted in Fig. 2. Our **contributions** are as follows:

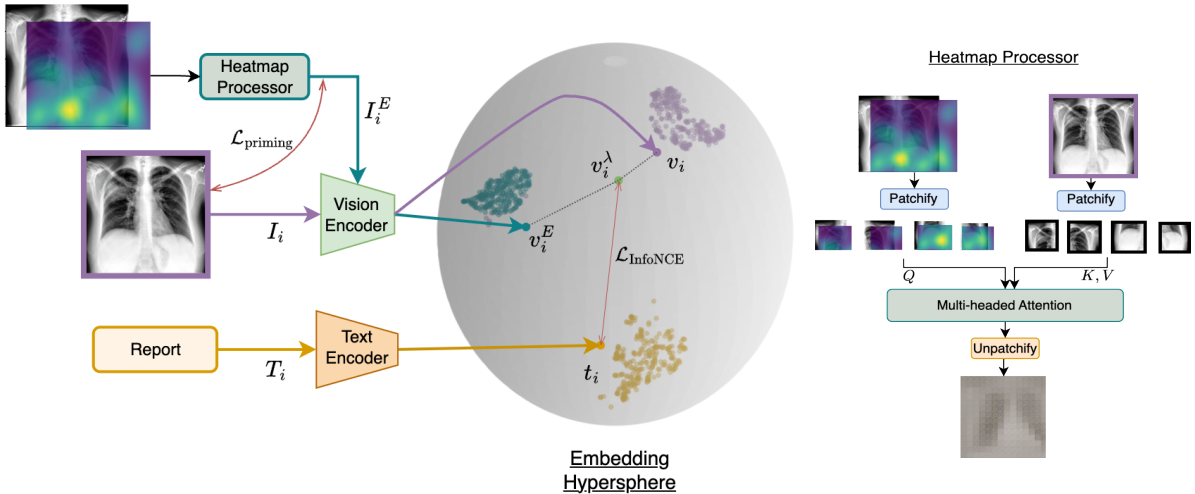


Figure 2: **eCLIP Pretraining with Expert Annotations.** eCLIP adds a Heatmap Processor (*right*), featuring a multi-headed attention layer, to the standard Image and Text encoders in CLIP. This processor, along with vision and text encoders, maps inputs into a shared hypersphere. Here, the original image (I_i), its text (T_i) and the heatmap-processed image (I_i^E) are positioned within a tripartite area (shown here after 2D UMAP projection, please refer to the Supplement for a scaled version). We employ mixup between I_i and I_i^E to generate the embedding v_i^λ , which gives us additional positive pairs to enhance the CLIP InfoNCE loss optimization. An auxiliary loss, $\mathcal{L}_{\text{priming}}$, is used during the initial training steps to “prime” the heatmap processor to imitate an identity function when the heatmap is composed of all ones.

- **Utilization of Expert Annotations.** We harness radiologist eye-gaze heatmaps to create additional embeddings, effectively introducing valuable positive and negative pairs for enhancing the contrastive learning process.
- **eCLIP Architecture.** Our implementation features a heatmap processing mechanism utilizing multi-headed attention (MHA), optimized for handling both heatmaps and original images. This is complemented by a mixup strategy to address the challenge of data scarcity, and curriculum learning to ensure a gradual introduction of expert annotations.
- **Comprehensive Evaluation.** We assess eCLIP’s zero-shot classification accuracy, sample efficiency and cross-modal retrieval performance and embedding quality across multiple chest X-ray datasets. We also evaluate the cross-modal embeddings to generate radiology reports using a frozen Large Language Model (LLM) without explicitly fine-tuning on medical data.

2 Related Work

Modality Gap: Liang et al. (2022) pinpoint the origins of the modality gap to the nuances of model initialization and the objectives of contrastive learning, underscoring its impact on downstream tasks and fairness. Oh et al. (2023) highlight poor uniformity and alignment in CLIP’s embeddings and propose a finetuning method for robust representations. Zhang et al. (2024) explore the geometry of this embedding space, and provide both theoretical and empirical insights on the nature of this geometry. Subsequent research has produced methods to mitigate the modality gap through diverse and creative approaches (Goel et al., 2022; Tschannen et al., 2023; Zhang et al., 2023b; Gu et al., 2023; Nukrai et al., 2022).

Improving Contrastive Learning: Several methods have improved upon the CLIP objective by introducing auxiliary losses, e.g., SLIP (Mu et al., 2022) uses SimCLR (Chen et al., 2020) loss, M3MAE (Geng et al.; Weers et al., 2023) augment the Masked Autoencoder (He et al., 2022) reconstruction loss, FLIP (Li et al., 2023) randomly masks out input images to improve scaling, DACL (Verma et al., 2021) proposes a

domain agnostic mixup strategy, SILC (Naeem et al., 2023) uses self-distillation, Mo et al. (2024) utilized specialist captions to generate pseudo labels for unpaired images, Zhang et al. (2023a) propose Multi-task Paired Masking with Alignment to improve cross-modal interaction. Similarly there have been works that have identified the need to make the CLIP model focus on sub-regions in order to enhance its utility and downstream performance, GLORIA (Huang et al., 2021) considers the loss from local regions from within the image and reports, Alpha-CLIP (Sun et al., 2023) uses the alpha channel to guide the CLIP model to focus on different regions of the image and generate the masks for all the images in the corpus using an image segmentation pipeline and TIER (Palepu & Beam, 2023) uses a regularization term to improve the local focus of the model.

Multi-modal Contrastive Learning in Medical Imaging: Zhang et al. (2022) demonstrated enhanced downstream performance by jointly using chest X-ray and report pairing for training a contrastive learning model. This was further improved by Huang et al. (2021), by exploiting local and global features from both modalities; Wang et al. (2022) and You et al. (2023) achieved impressive results by using a Swin Tiny model as the image encoder and by adding modifications to the contrastive loss. Several other works have developed similar contrastive learning foundation models while utilizing the biomedical image texts to achieve impressive results (Huang et al., 2023; Xu et al., 2023b; Moor et al., 2023; Wu et al., 2023; Sowrirajan et al., 2010; Tu et al., 2024). Karagyris et al. (2021) and Bigolin Lanfredi et al. (2022) augment a subset of the MIMIC-CXR (Johnson et al., 2019b) samples with high quality eye-tracking and verbal transcripts from several radiologists. van Sonsbeek et al. (2023) and Wang et al. (2024) utilize the heatmaps from eye-gaze to improve image classification.

3 Method

Notations. For a given chest X-ray image I_i and its radiology report T_i , indexed by i in our dataset, we denote their L2-normalized embeddings as v_i and t_i respectively, residing in a d -dimensional space ($v_i, t_i \in \mathcal{R}^d$). Image embeddings are obtained through an encoder $v_i = f(I_i)$ and text embeddings via $t_i = g(T_i)$. Applying an expert heatmap E_i to an image results in the corresponding image embedding v_i^E . We denote the loss value for the i -th sample as \mathcal{L}_i . For the case of contrastive loss, this is computed in terms of some similarity measure between the embeddings, $sim(v_i, t_i)$, typically cosine similarity defined as $v_i \cdot t_i$.

3.1 Background

Central to CLIP’s effectiveness is the InfoNCE loss (Oord et al., 2018), a mechanism engineered to optimize the similarity measures between corresponding (positive) pairs and to minimize those among non-corresponding (negative) pairs. The formulation of the CLIP loss objective is as follows:

$$\mathcal{L}_{\text{text}} = \mathbb{E}_{(t_i, v_i) \sim \text{pos}} \left[-\log \frac{\exp(sim(t_i, v_i)/\tau)}{\exp(sim(t_i, v_i)/\tau) + \sum_{j \neq i} \exp(sim(t_i, v_j)/\tau)} \right] \quad (1)$$

Total loss is then defined as, $\mathcal{L}_{\text{total}} = \frac{1}{2} (\mathcal{L}_{\text{text}} + \mathcal{L}_{\text{image}})$, where $\mathcal{L}_{\text{image}}$ denotes the corresponding loss for the image to text mapping. Here, τ represents the temperature parameter that controls the scale of the similarity scores, typically framed as a learnable parameter during training. The loss expectation is taken over all the positive pairings in the dataset.

Theoretical results on CL indicate the concepts of *alignment* and *uniformity* as critical for the quality of embeddings (Wang & Isola, 2020; Wang & Liu, 2021). Alignment focuses on reducing the distance between positive pairs while uniformity seeks to evenly distribute the embeddings across the unit hypersphere, preventing extreme clustering that could impair the model’s generalizability and discriminative capabilities. The alignment and uniformity can be defined formally as follows (Oh et al., 2023):

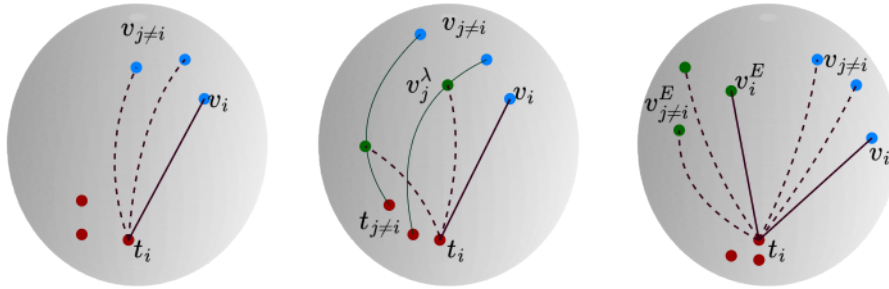


Figure 3: **Comparing eCLIP with m^2 -mixup(Oh et al., 2023).** (*left*) Standard CLIP showing image-text positive pairs (v_i, t_i) (solid line), while the other image embeddings serve as negative pairs (dashed line). (*center*) the m^2 -mixup creates negative pairs (v_j^λ, t_i) via interpolation between embeddings along the geodesic. (*right*) eCLIP adds expert image embedding, v_i^E , in addition to v_i for text t_i , forming additional positive and negative pairs

$$\text{Alignment} = -\mathbb{E}_{(v_i, t_i) \sim \text{pos}} \left[\|v_i - t_i\|_2^2 - \min_{j \neq i} \|v_i - t_j\|_2^2 \right] \quad (2)$$

$$\text{Uniformity} = -\log \mathbb{E}_{(v_i, t_j) \sim \mathcal{D}} \left[\exp(-2\|v_i - t_j\|_2^2) \right] \quad (3)$$

High intra-modal similarity, e.g. between two images as seen in Fig. 1, can inadvertently enhance similarity among negative pairs, inflating the denominator of the loss function in Equation (1), and, consequently, hurting the model’s ability to differentiate between positive and negative pairs during training. A conventional method to counter this involves incorporating hard negative pairs, a strategy (Oh et al., 2023) employ by mixing embeddings from different modalities. While effective, this cross-modal mixup may obscure the semantic clarity of embeddings. As an alternative we propose increasing the dataset with additional positive pairs that exhibit minimal semantic overlap by integrating expert annotations. Fig. 3 compares the positive and negative pair creation in eCLIP with traditional CLIP and m^2 -mixup.

3.2 Introducing Expert Annotations to CLIP

Our objective with eCLIP is to enhance the CLIP framework by integrating expert annotations – radiologist eye-gaze heatmaps – to diversify the pool of positive samples. The eCLIP model is designed to be compatible across all CLIP variants without modifying its core architecture. The **heatmap processor** (Fig. 2, *right*) first converts the images and heatmaps into a sequence of patches and applies multi-headed attention (MHA) over the sequences. The patchified heatmap overlaid images serve as queries, while the original image’s patches act as keys and values. The processed output is then reconstructed back to its original image format, enabling the standard CLIP image encoder to obtain expert image embeddings. These new embeddings and their text embedding pair introduce additional positive samples for the contrastive loss objective (Fig. 3, *right*).

However, the size of the expert annotated data is orders of magnitude smaller than the data available for CLIP training. To effectively leverage the scarce expert-annotated data, we implement **mixup** augmentation (Zhang et al., 2017). As illustrated in Fig. 2 (*left*), this involves blending an original image I_i with its expert version I_i^E to create $I_i^\lambda = \lambda I_i + (1 - \lambda)I_i^E$, where $\lambda \sim \text{Beta}(\alpha, \alpha)$. (We set $\alpha = 0.3$ in all our experiments.) The eCLIP image encoder then processes I_i^λ to produce the image embedding $v_i^\lambda = f(I_i^\lambda)$. These expert embeddings form new positive pairs (v_i^λ, t_i) as well as corresponding negative pairs, which are added with existing pairs (v_i, t_i) during the computation of the CLIP InfoNCE Loss, \mathcal{L}_i .

To seamlessly integrate expert annotations without disrupting the foundational training of the eCLIP model, we employ a phased **curriculum learning** strategy (Bengio et al., 2009). This approach comprises a cold start phase where the model is initially trained without the expert annotations to establish a robust baseline.

Algorithm 1 eCLIP Algorithm

Require: Image Encoder $f(\cdot)$ **Require:** Text Encoder $g(\cdot)$

```
1:  $\mathcal{L}_{\text{priming}} \leftarrow 0$ ;  $n_p \leftarrow 0$ 
2: for minibatch  $\{x_i\}_{i=1}^N$  do
3:   Unpack  $x_i$  to  $(T_i, I_i)$  and optionally  $E_i$ 
4:    $t_i \leftarrow g(T_i)$ 
5:    $v_i \leftarrow f(I_i)$ 
6:    $p_{\text{uni}} \sim \text{Uniform}(0, 1)$ 
7:   if  $p_{\text{uni}} < p_{\text{curr}}$  and  $E_i$  is provided then
8:      $\lambda \sim \text{Beta}(\alpha, \alpha)$ 
9:      $I_i^E \leftarrow \text{HeatmapProcessor}(I_i, E_i)$ 
10:     $I_i^\lambda \leftarrow I_i \lambda + I_i^E (1 - \lambda)$ 
11:     $v_i^\lambda \leftarrow f(I_i^\lambda)$ 
12:  end if
13:  if  $E_i$  is entirely ones then
14:     $I_i^R \leftarrow \text{HeatmapProcessor}(I_i, E_i)$ 
15:     $\mathcal{L}_{\text{priming}} \leftarrow \mathcal{L}_{\text{priming}} + (I_i - I_i^R)^2$ 
16:     $n_p \leftarrow n_p + 1$ 
17:  end if
18: end for
```

// Compute Total Loss

Require: Temperature τ $V \leftarrow$ List of v_i for all i $T \leftarrow$ List of t_i for all i **for** $i = 1$ **to** N **do** **if** v_i^λ exists **then** $V \leftarrow \text{Append}(V, v_i^\lambda)$ $T \leftarrow \text{Append}(T, t_i)$ **end if****end for** $\mathcal{L}_{\text{clip}} \leftarrow \text{ClipLoss}(V, T, \tau)$ **if** $n_p > 0$ **then** $\mathcal{L}_{\text{priming}} \leftarrow \frac{1}{n_p} \mathcal{L}_{\text{priming}}$ **end if** $\mathcal{L}_{\text{total}} \leftarrow (1 - w_p) \cdot \mathcal{L}_{\text{clip}} + w_p \cdot \mathcal{L}_{\text{priming}}$ **Hyperparameters:**

- Batch size N
 - Mixup Alpha α
 - Curriculum Prob. p_{curr}
 - MSE Loss weight w_p
-

This phase accounts for about 10% of the total training iterations. It then transitions into a warmup phase, gradually increasing the inclusion of expert examples from 0.05 to 0.5 probability over the next 30% of iterations. Finally, a cooldown phase reduces expert example probability to 0.1 for the subsequent 40% of iterations, fine-tuning the model’s performance by balancing foundational and expert-driven insights.

Additionally, we regularize the heatmap processor to behave as an identity function in scenarios where the heatmap is entirely composed of ones. We achieve this through a **priming** phase that coincides with the curriculum learning’s cold start phase. We setup an auxillary mean-squared error loss to force the heatmap processor to reconstruct the original image I_i when the heatmap $E_i = 1$. This priming ensures the heatmap processor’s adaptability, allowing it to process expert annotations effectively when available, while falling back to the model’s original performance in their absence. The total loss during this phase is, $\mathcal{L}_{\text{total}} = w_p \cdot \mathcal{L}_{\text{priming}} + (1 - w_p) \cdot \mathcal{L}_{\text{clip}}$, where w_p is a hyperparameter which we set to 0.1. The pseudocode for eCLIP is shown in Algorithm 1.

4 Experiments

Our experiments are designed to evaluate the influence of expert heatmap annotations on the quality of the learned representations. Unless stated otherwise, we assume that a large set of image-text pairs, of which a small fraction is annotated with eye-gaze heatmaps, is used for training, but for test samples no annotations are used. We utilize both quantitative measures and qualitative assessments to study the contributions of these annotations towards enhancing model performance.

4.1 Setup

4.1.1 Baselines

To validate our approach, we compare eCLIP against a model trained using traditional CLIP (referred to as the base model) and a “naive” baseline, where the expert annotated samples are directly added to the training set without using mixup or curriculum learning. We also examine the impact of two mixup methods: Domain Agnostic Contrastive Learning (DACL) (Verma et al., 2021) and m^3 -mixup (Oh et al., 2023) which

blends image and text embeddings to improve alignment and uniformity across modalities. While DACL is integrated during pretraining, m^3 -mixup is applied post-pretraining, in a manner akin to fine-tuning. eCLIP can be applied to any variant of CLIP, which we demonstrate also with GLoRIA (Huang et al., 2021) which has a Resnet50 image encoder. We introduce **two variants** of our technique: eCLIP, which integrates expert annotations during the initial CLIP pretraining phase, and eCLIP^P, which instead continually finetunes a trained CLIP model with expert annotations, similar to m^3 -mixup.

4.1.2 Datasets

For pretraining phase we utilize the **MIMIC-CXR** dataset (Johnson et al., 2019b), which pairs roughly 200K chest X-rays with free-text radiology reports. The images were processed into JPEG format as described in (Johnson et al., 2019a), and the accompanying reports were stripped of unnecessary punctuation and tokenized using the Wordpiece scheme (Devlin et al., 2018). We obtain the eye-gaze heatmap from the EGD-CXR dataset (Demner-Fushman et al., 2016) and process the eye-tracking data to obtain the normalized eye-gaze heatmap which are available for 1080 datapoints.

Our evaluation setup includes multiple publicly available chest X-ray datasets, specifically **CheXpert** (Irvin et al., 2019), **RSNA Pneumonia** (Shih et al., 2019), **NIH CXR** (Wang et al., 2017) and **Open-I** (Demner-Fushman et al., 2016), each offering a distinct set of imaging and reporting characteristics. Following previous works (Wang et al., 2022; Huang et al., 2021; You et al., 2023), we prepare the test sets from MIMIC and CheXpert, selecting 200 random samples for five specific pathologies from the CheXpert competition, resulting in 1000 samples for each dataset (MIMIC 5x200 and CheXpert 5x200, respectively). For the NIH-CXR dataset, we assembled a subset of 100 samples for each of 14 abnormalities, thereby creating CXR 14x100 test set. The Open-I dataset is utilized for text retrieval and radiology report generation tasks. For linear probe evaluations, we use CXR-8 (Wang et al., 2017), RSNA dataset and construct an OpenI-5 dataset by extracting labels from the ‘Problems’ field within the reports that match the CheXpert competition labels.

4.1.3 Training

We employed CLIP pretraining on the MIMIC-CXR dataset, utilizing a subset with roughly 1000 images with expert eye-gaze heatmap annotations, while validation and all other downstream evaluations proceed without these annotations. Our model architecture includes Swin Tiny, following recent studies (Wang et al., 2022; You et al., 2023), alongside Vision Transformer (ViT) Small and Base, with image encoders pretrained on ImageNet and Clinical BERT (Alsentzer et al., 2019) with max length of sequences set to 256 as the text encoder. We cropped images to (224, 224) using random resized crop augmentation and turned off all other image augmentations. Pretraining utilized 8 AMD MI250X GPUs, maintaining an effective batch size of 512 for 10,000 steps. The learning rate was $1e^{-4}$ for standard CLIP, increased to $2e^{-4}$ for eCLIP variants, with cosine annealing plus a linear warmup for the first 10% of iterations, weight decay of $1e^{-3}$, and learnable temperature parameter in the contrastive loss initialized at 0.07. Models for m^3 -mixup and eCLIP^P are initialized with weights from CLIP pretraining and further finetuned for 1,000 iterations with a learning rate of $1e^{-5}$. Detailed setup information is available in the Supplement.

4.2 Zero-shot Image Classification

Following CLIP (Radford et al., 2021), our zero-shot classification method categorizes images into predefined classes without direct finetuning, thus relying on the quality of embeddings generated during pretraining. To formulate the embedding of each class label, we first generate descriptive prompts to obtain a list of text embeddings corresponding to the label using the text encoder (Huang et al., 2021; Wang et al., 2022; You et al., 2023). The mean of these embeddings is taken as the representation of the label. For each image, classification is then performed by matching the image embedding with its closest label embedding through cosine similarity. More details of the prompts used are provided in the Supplement.

Table 1 illustrates the zero-shot classification performance on CheXpert 5x200, MIMIC 5x200, RSNA, and CXR 14x100 datasets. The results, based on macro-averaged F1 scores from three random initializations, highlight eCLIP variants’ superior performance over the base models across all datasets. While the m^3 -mixup excels in MIMIC for certain architectures, eCLIP variants show broader generalization. Notably, eCLIP’s

Table 1: Zero-shot classification performance on 4 X-ray datasets and model configurations, reported as macro-averaged F1 scores from three independent random seeds. The highest score per dataset and model configuration is underlined. The overall best-performing model for each dataset is highlighted in bold.

Model	Dataset			
	CheXpert 5x200	MIMIC 5x200	RSNA	CXR 14x100
GLoRIA _{Resnet50}	0.478 \pm .023	0.457 \pm .016	0.736 \pm .024	0.155 \pm .001
+naive	0.391 \pm .069	0.334 \pm .057	0.731 \pm .023	0.113 \pm .024
+DACL	0.506 \pm .029	0.430 \pm .011	0.736 \pm .007	0.158 \pm .004
+ m^3 -mix	<u>0.512\pm.005</u>	0.467 \pm .004	0.760 \pm .006	<u>0.160\pm.003</u>
+expert (ours)	0.507 \pm .004	0.430 \pm .009	<u>0.761\pm.017</u>	0.156 \pm .023
+expert ^P (ours)	0.507 \pm .005	<u>0.475\pm.008</u>	0.775 \pm .001	0.159 \pm .001
CLIP _{Swin Tiny}	0.517 \pm .025	0.452 \pm .002	0.808 \pm .000	0.169 \pm .003
+naive	0.532 \pm .010	0.452 \pm .022	0.807 \pm .007	0.167 \pm .007
+DACL	0.465 \pm .008	0.389 \pm .015	0.768 \pm .018	0.101 \pm .013
+ m^3 -mix	0.554 \pm .006	<u>0.469\pm.008</u>	0.802 \pm .004	0.179 \pm .008
+expert (ours)	0.549 \pm .016	0.445 \pm .021	0.818 \pm .004	0.172 \pm .006
+expert ^P (ours)	<u>0.558\pm.004</u>	0.463 \pm .007	0.819\pm.000	<u>0.192\pm.003</u>
CLIP _{ViT Small}	0.525 \pm .024	0.441 \pm .006	0.807 \pm .006	0.159 \pm .007
+naive	0.534 \pm .016	0.440 \pm .019	0.805 \pm .004	0.156 \pm .017
+DACL	0.475 \pm .025	0.398 \pm .015	0.761 \pm .009	0.133 \pm .007
+ m^3 -mix	0.557 \pm .002	<u>0.454\pm.003</u>	0.809 \pm .002	0.164 \pm .002
+expert (ours)	0.545 \pm .016	<u>0.452\pm.013</u>	0.803 \pm .003	0.165 \pm .007
+expert ^P (ours)	<u>0.559\pm.001</u>	0.439 \pm .004	<u>0.817\pm.001</u>	<u>0.165\pm.004</u>
CLIP _{ViT Base}	0.540 \pm .017	0.465 \pm .004	0.805 \pm .001	0.183 \pm .011
+naive	0.506 \pm .011	0.426 \pm .006	0.805 \pm .004	0.151 \pm .009
+DACL	0.474 \pm .007	0.400 \pm .002	0.759 \pm .001	0.106 \pm .003
+ m^3 -mix	0.542 \pm .021	0.465 \pm .013	0.798 \pm .004	0.183 \pm .020
+expert (ours)	<u>0.563\pm.021</u>	<u>0.477\pm.004</u>	<u>0.814\pm.003</u>	<u>0.193\pm.017</u>
+expert ^P (ours)	0.549 \pm .003	0.452 \pm .007	0.810 \pm .001	0.185 \pm .002

advantages are more pronounced in multi-class scenarios (CheXpert, MIMIC and CXR14) compared to binary classification on RSNA.

4.3 Sample Efficiency

Sample efficiency measures how well a model learns from limited amount of training data. eCLIP improves this efficiency by using expert annotated images to form new positive and negative pairs, aiming to improve the quality of the learned embeddings. To test this, we first looked at zero-shot classification performance, adjusting the number of training batches available for pretraining. Results, shown in Fig. 4 (*top row*), reveal that eCLIP is more sample efficient across MIMIC 5x200, CheXpert 5x200 and CXR 14x100 datasets compared to the base model. Additionally, by applying supervised fine-tuning (SFT) with a linear probe on class-imbalanced datasets – CXR-8, RSNA and OpenI-5 (Section 4.1.2) – eCLIP demonstrates stronger performance in multi-label classification tasks, CXR-8 and OpenI-5 and remains competitive in binary classification for RSNA. This is shown Fig. 4 (*bottom row*) where we plot the ROC AUC scores against different training sample sizes for linear probing. These findings highlight eCLIP’s ability to effectively learn from fewer samples.

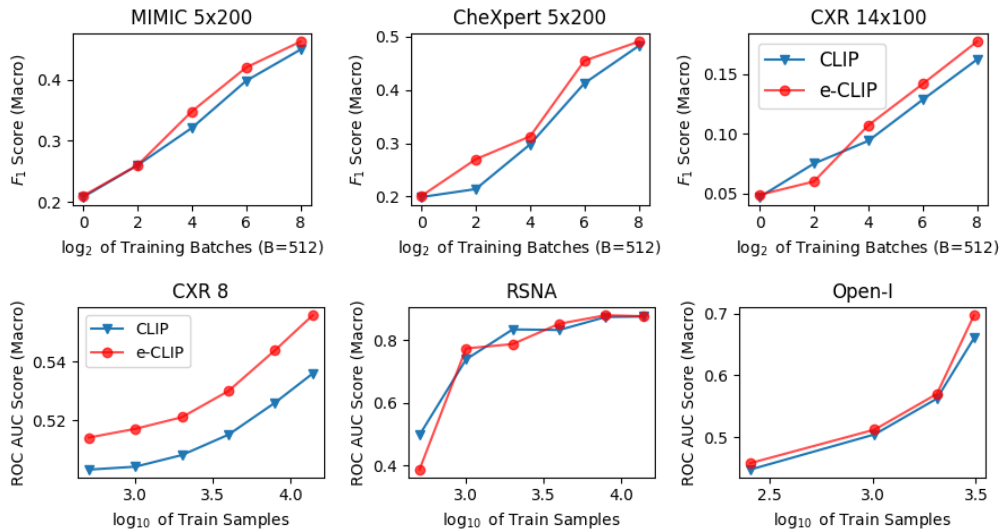


Figure 4: **Sample Efficiency.** (*top row*) Zero-shot performance on three multi-label classification test sets for CLIP and eCLIP Swin Tiny models, trained with varying amounts of training batches. (*bottom row*) Linear probe scores with varying amounts of training data.

Table 2: Performance on Image to Report retrieval with Open-I dataset. We report the Recall@{1, 5, 10}

Model	R@1	R@5	R@10
CLIP _{Swin Tiny}	3.1	7.6	11.3
+ m^3 -mix	2.4	6.5	9.8
+expert (ours)	<u>3.7</u>	<u>9.4</u>	<u>13.4</u>
+expert ^P (ours)	3.1	8.2	11.7
CLIP _{ViT Base}	3.7	9.2	13.2
+ m^3 -mix	4.1	8.8	13.0
+expert (ours)	<u>4.4</u>	<u>10.3</u>	<u>13.5</u>
+expert ^P (ours)	2.9	7.5	10.3

Table 3: Performance on report generation with Open-I dataset. We report the BLEU-2 score (BL-2), BERT recall score(Zhang et al., 2019) (B-R), Cosine similarity between the sentence embeddings of the generated and ground-truth report for MP-Net (Song et al., 2020) Sentence Transformer model (Reimers & Gurevych, 2019) (S_{emb}), and for the CheXBERT model(Smit et al., 2020) (CB_{emb})

Model	BL-2	B-R	S_{emb}	CB_{emb}
CLIP	0.172	0.713	0.791	0.492
eCLIP	0.177	0.712	0.795	0.506

Table 4: **Ablation Study with Swin Tiny.** Zero-shot performance on CheXpert (CXP) and CXR14 (C14) datasets for the base CLIP and models with expert annotation integration (+E) is presented. Methods include mask multiplication (\odot), CNN, and Multi-headed Attention (MHA) encoders. Key augmentations: Mixup (+M), Curriculum Learning (+C), and Encoder Priming (+P) demonstrate performance gains. A control with a random mask (*rand*) confirms the significance of expert annotations. We report macro-averaged F1 scores from three random initialization

Method	CXP	C14
Base	0.517 \pm .024	0.169 \pm .003
\odot Mask (+ E)	0.540 \pm .019	0.165 \pm .006
CNN Encoder (+ E)	0.534 \pm .012	0.163 \pm .008
MHA Encoder (+ E)	0.534 \pm .013	0.153 \pm .002
MHA Encoder (+ E, M)	0.532 \pm .018	0.160 \pm .010
MHA Encoder (+ E, M, C)	0.545 \pm .008	0.173 \pm .018
MHA Encoder (+ rand, M, C, P)	0.537 \pm .020	0.166 \pm .003
MHA Encoder (+ E, M, C, P)	0.549 \pm .016	0.172 \pm .006

Table 5: **Random samples of generated report.** For each image in the Open-I dataset, the five closest text snippets based on embedding cosine similarity is used as prompts for Mistral 7B LLM. Utilizing in-context learning, we prompt the LLM with two such snippet-report pairs. The conditions that the generated report identified correctly are highlighted in green while those it missed are shown in red.

Problems	Ground Truth	Generated
normal	The lungs and pleural spaces show no acute abnormality. Heart size and pulmonary vascularity within normal limits.	The lungs are clear with no evidence of consolidation, pneumothorax, or pleural effusion. Heart size and mediastinal contour are normal. No acute abnormalities noted in the visualized osseous structures.
Pulmonary Atelectasis. Pleural Effusion. Cardiomegaly. Pulmonary Congestion	AP and lateral views were obtained. Bibasilar atelectasis and small left-sided pleural effusion. Stable cardiomegaly. No pneumothorax. Mild pulmonary vascular congestion.	The lungs show bibasilar airspace opacities, possibly due to infection or atelectasis. Heart size is mildly enlarged. No pneumothorax or pleural effusion.
Lung. Density. Emphysema	There is hyperexpansion. The heart size is normal. There is no pleural effusion or pneumothorax. Two circular densities overlying the right ribs which were not present in the XXXX CT. No focal infiltrates	The lungs are hyperexpanded with clear fields and no acute consolidations or pleural effusions. Heart size and pulmonary vascularity are within normal limits. Degenerative changes are present in the thoracic spine. A calcified granuloma is noted in the left perihilar region. No pneumothorax or large pleural effusion is observed.

4.4 Text retrieval and retrieval augmented generation (RAG)

To compare eCLIP’s cross-modal functionality with that of CLIP we focused on text retrieval task using the Open-I dataset, which consists of pairs of X-rays and radiology reports. We used the FAISS vector database (Douze et al., 2024) to index the text embeddings generated by the text encoder. For a given X-ray image I_i , we then retrieve the closest text reports from the database based on the cosine similarity in the embedding space, $\min_j(v_i \cdot t_j)$. Results in Table 2 compare the performance of eCLIP against CLIP in text retrieval measured in Recall@1, 5, and 10. The performance of eCLIP indicates a notable improvement in its embedding quality. Note that our evaluation followed a strict criterion for recall computation, where a retrieval was counted as successful only if the exact correct report was identified. While more nuanced measures based on semantic similarity could be employed (You et al., 2023), we opted this approach to maintain a clear and simple evaluation framework.

Next we extend our analysis from retrieval to report generation using a frozen Large Language Model (LLM), Mistral 7B Instruct v2 (Jiang et al., 2023), aiming to generate radiology reports through Retrieval Augmented Generation (RAG). This setup tests the CLIP model’s capacity to retrieve texts which can be used to prompt an LLM to generate a report without finetuning on medical data. First we randomly selected 389 samples from the Open-I dataset for testing and utilized the FAISS database to index the reports from the remaining samples (i.e., training set). Given a test image we retrieve five closest reports from the training set and use them in the prompt for the LLM to generate a report for the test image. The eCLIP variant showed a small but consistent improvement over the base model in generating reports, as indicated in Table 3. A comparative analysis of generated report versus ground truth shown in Table 5, with discrepancies

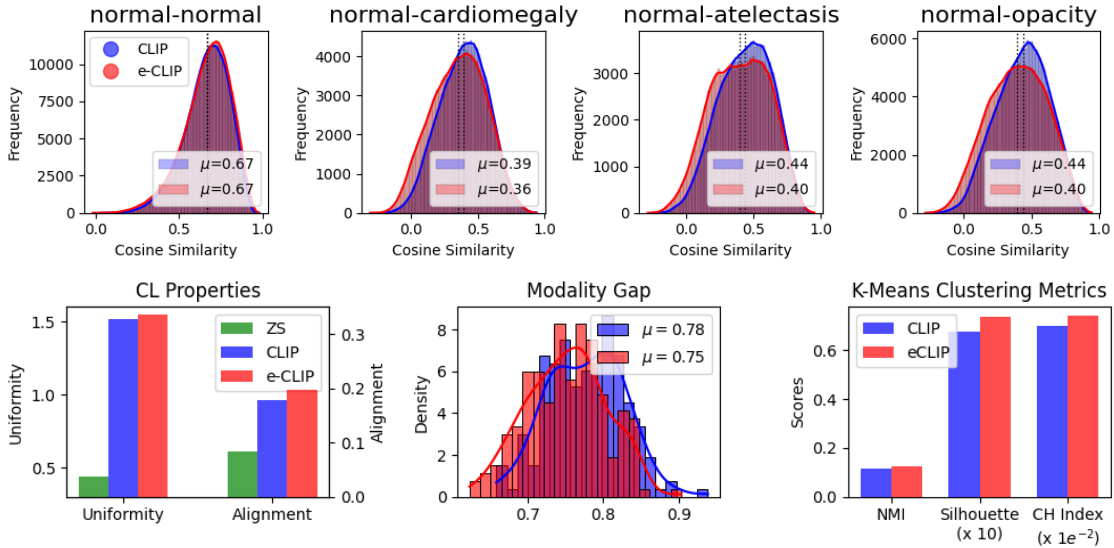


Figure 5: **Qualitative Analysis of CLIP Pretraining.** *top row* illustrates the cosine similarity distributions for CLIP and eCLIP image embeddings. *bottom left and center* sections display uniformity, alignment, and modality gap comparisons among the internet pretrained model (ZS), CLIP pretrained on MIMIC, and eCLIP. *bottom right* details K-means clustering metrics for image embeddings with $k=5$ for both CLIP and eCLIP models.

marked, further validates the effectiveness of eCLIP’s embeddings in supporting complex cross-modal tasks. Additional details, including LLM prompts and generated report samples are available in the Supplement.

4.5 Embedding Quality

For qualitative evaluations, we first examine the histogram of the cosine similarities of the embeddings from different abnormality subgroups obtained from the CLIP image encoder. In Fig. 5 (*top row*), we can see that the similarities for the CLIP model has considerably dropped below 1 after continual pretraining on MIMIC-CXR compared to Fig. 1. This indicates that the model’s ability to distinguish between different conditions has improved. The introduction of expert annotations in the eCLIP variant further improves this with mean cosine similarities for ‘normal’ versus cardiomegaly, atelectasis and opacity dropping to 0.36, 0.4 and 0.4 respectively.

Our evaluation of uniformity and alignment reveals that eCLIP surpasses both the MIMIC-pretrained and internet-pretrained models in these key metrics, indicating a marked improvement in the quality of embeddings (Fig. 5, *bottom left*). We also note a modest decrease in the modality gap with eCLIP (Fig. 5, *bottom center*). Clustering analysis via K-means (with $k=5$ for 5 abnormalities in data) highlights eCLIP’s superior performance in grouping abnormalities, as seen from improved scores in Normalized Mutual Information (NMI), Silhouette score, and Calinski-Harabasz (CH) index (Fig. 5, *bottom right*).

4.6 Ablation Study

Our ablation study with the Swin Tiny encoder shows the impact of key components in our eCLIP model: multi-headed attention (MHA) layer for heatmap processing, curriculum learning for phased introduction of expert annotations, mixup augmentation to compensate for limited number of expert annotated data and priming of heatmap processor during initial training phase. Results shown in Table 4 reveal that the MHA-based heatmap processor improves zero-shot classification performance on CheXpert 5x200 and CXR 14x100 datasets compared to basic methods like direct application of heatmaps as mask ($\odot Mask$) or using a CNN encoder. We note a significant performance drop with randomly generated heatmaps versus expert eye-gaze

heatmaps. This highlights that while our methodological improvements contribute to the performance gains, the integration of meaningful, expert-derived signals is essential for achieving optimal results.

5 Conclusion

We introduce eCLIP, an adaptation of CLIP, demonstrating the integration of radiologist eye-tracking heatmap to overcome challenges faced in multi-modal contrastive learning. This study highlights the impact of integrating these high-quality expert annotations on improving the quality of learned embeddings and assess its influence on sample efficiency and cross-modal retrieval tasks. An important future research direction would be extending this approach to include expert annotations from the text modality (e.g., by adapting SimCSE (Gao et al., 2021)) and to leverage the temporal dynamics of eye-tracking data by aligning the sequential frames with the corresponding report snippets.

5.0.1 Limitations

Our study is limited by the small size of expert annotated data and thus does not comprehensively analyze the impact of size or distribution of expert annotations across different abnormalities. eCLIP also incurs extra computational costs during training due to the additional forward pass required for processing expert images in the warmup and cool-down phases. Additionally, the clinical relevance of generated radiology reports has not been validated by medical experts, relying instead on standard metrics known for potential biases and inaccuracies in reflecting clinical accuracy (Yu et al., 2023).

References

- Emily Alsentzer, John R Murphy, Willie Boag, Wei-Hung Weng, Di Jin, Tristan Naumann, and Matthew McDermott. Publicly available clinical BERT embeddings. *arXiv preprint arXiv:1904.03323*, 2019.
- Yoshua Bengio, Jérôme Louradour, Ronan Collobert, and Jason Weston. Curriculum learning. In *Proceedings of the 26th annual international conference on machine learning*, pp. 41–48, 2009.
- Ricardo Bigolin Lanfredi, Mingyuan Zhang, William F Auffermann, Jessica Chan, Phuong-Anh T Duong, Vivek Srikumar, Trafton Drew, Joyce D Schroeder, and Tolga Tasdizen. Reflax, a dataset of reports and eye-tracking data for localization of abnormalities in chest x-rays. *Scientific data*, 9(1):350, 2022.
- Ting Chen, Simon Kornblith, Mohammad Norouzi, and Geoffrey Hinton. A simple framework for contrastive learning of visual representations. In *International conference on machine learning*, pp. 1597–1607. PMLR, 2020.
- Mehdi Cherti, Romain Beaumont, Ross Wightman, Mitchell Wortsman, Gabriel Ilharco, Cade Gordon, Christoph Schuhmann, Ludwig Schmidt, and Jenia Jitsev. Reproducible scaling laws for contrastive language-image learning. In *Proceedings of the IEEE/CVF Conference on Computer Vision and Pattern Recognition*, pp. 2818–2829, 2023.
- Dina Demner-Fushman, Marc D Kohli, Marc B Rosenman, Sonya E Shooshan, Laritza Rodriguez, Sameer Antani, George R Thoma, and Clement J McDonald. Preparing a collection of radiology examinations for distribution and retrieval. *Journal of the American Medical Informatics Association*, 23(2):304–310, 2016.
- Jacob Devlin, Ming-Wei Chang, Kenton Lee, and Kristina Toutanova. BERT: Pre-training of deep bidirectional transformers for language understanding. *arXiv preprint arXiv:1810.04805*, 2018.
- Matthijs Douze, Alexandr Guzhva, Chengqi Deng, Jeff Johnson, Gergely Szilvasy, Pierre-Emmanuel Mazaré, Maria Lomeli, Lucas Hosseini, and Hervé Jégou. The faiss library. *arXiv preprint arXiv:2401.08281*, 2024.
- Tianyu Gao, Xingcheng Yao, and Danqi Chen. SimCSE: Simple contrastive learning of sentence embeddings. *arXiv preprint arXiv:2104.08821*, 2021.
- Xinyang Geng, Hao Liu, Lisa Lee, Dale Schuurmans, Sergey Levine, and Pieter Abbeel. M3ae: Multimodal masked autoencoders learn transferable representations. Technical report, Technical Report.

-
- Shashank Goel, Hritik Bansal, Sumit Bhatia, Ryan Rossi, Vishwa Vinay, and Aditya Grover. CyCLIP: Cyclic contrastive language-image pretraining. *Advances in Neural Information Processing Systems*, 35: 6704–6719, 2022.
- Sophia Gu, Christopher Clark, and Aniruddha Kembhavi. I can’t believe there’s no images! learning visual tasks using only language supervision. In *Proceedings of the IEEE/CVF International Conference on Computer Vision*, pp. 2672–2683, 2023.
- Zongbo Han, Zhipeng Liang, Fan Yang, Liu Liu, Lanqing Li, Yatao Bian, Peilin Zhao, Bingzhe Wu, Changqing Zhang, and Jianhua Yao. Umix: Improving importance weighting for subpopulation shift via uncertainty-aware mixup. *Advances in Neural Information Processing Systems*, 35:37704–37718, 2022.
- Kaiming He, Xinlei Chen, Saining Xie, Yanghao Li, Piotr Dollár, and Ross Girshick. Masked autoencoders are scalable vision learners. In *Proceedings of the IEEE/CVF conference on computer vision and pattern recognition*, pp. 16000–16009, 2022.
- Shih-Cheng Huang, Liyue Shen, Matthew P Lungren, and Serena Yeung. Gloria: A multimodal global-local representation learning framework for label-efficient medical image recognition. In *Proceedings of the IEEE/CVF International Conference on Computer Vision*, pp. 3942–3951, 2021.
- Zhi Huang, Federico Bianchi, Mert Yuksekogul, Thomas J Montine, and James Zou. A visual–language foundation model for pathology image analysis using medical twitter. *Nature medicine*, 29(9):2307–2316, 2023.
- Jeremy Irvin, Pranav Rajpurkar, Michael Ko, Yifan Yu, Silviana Ciurea-Ilcus, Chris Chute, Henrik Marklund, Behzad Haghgoo, Robyn Ball, Katie Shpanskaya, et al. CheXpert: A large chest radiograph dataset with uncertainty labels and expert comparison. In *Proceedings of the AAAI conference on artificial intelligence*, volume 33, pp. 590–597, 2019.
- Chao Jia, Yinfei Yang, Ye Xia, Yi-Ting Chen, Zarana Parekh, Hieu Pham, Quoc Le, Yun-Hsuan Sung, Zhen Li, and Tom Duerig. Scaling up visual and vision-language representation learning with noisy text supervision. In *International conference on machine learning*, pp. 4904–4916. PMLR, 2021.
- Albert Q Jiang, Alexandre Sablayrolles, Arthur Mensch, Chris Bamford, Devendra Singh Chaplot, Diego de las Casas, Florian Bressand, Gianna Lengyel, Guillaume Lample, Lucile Saulnier, et al. Mistral 7B. *arXiv preprint arXiv:2310.06825*, 2023.
- Alistair Johnson, Matt Lungren, Yifan Peng, Zhiyong Lu, Roger Mark, Seth Berkowitz, and Steven Horng. MIMIC-CXR-JPG-Chest radiographs with structured labels. *PhysioNet*, 2019a.
- Alistair EW Johnson, Tom J Pollard, Seth J Berkowitz, Nathaniel R Greenbaum, Matthew P Lungren, Chihying Deng, Roger G Mark, and Steven Horng. MIMIC-CXR, a de-identified publicly available database of chest radiographs with free-text reports. *Scientific data*, 6(1):317, 2019b.
- Alexandros Karargyris, Satyananda Kashyap, Ismini Lourentzou, Joy T Wu, Arjun Sharma, Matthew Tong, Shafiq Abedin, David Beymer, Vandana Mukherjee, Elizabeth A Krupinski, et al. Creation and validation of a chest X-ray dataset with eye-tracking and report dictation for AI development. *Scientific Data*, 8(1): 92, 2021.
- Rayan Krishnan, Pranav Rajpurkar, and Eric J Topol. Self-supervised learning in medicine and healthcare. *Nature Biomedical Engineering*, 6(12):1346–1352, 2022.
- Yanghao Li, Haoqi Fan, Ronghang Hu, Christoph Feichtenhofer, and Kaiming He. Scaling language-image pre-training via masking. In *Proceedings of the IEEE/CVF Conference on Computer Vision and Pattern Recognition*, pp. 23390–23400, 2023.
- Victor Weixin Liang, Yuhui Zhang, Yongchan Kwon, Serena Yeung, and James Y Zou. Mind the gap: Understanding the modality gap in multi-modal contrastive representation learning. *Advances in Neural Information Processing Systems*, 35:17612–17625, 2022.

-
- Haotian Liu, Chunyuan Li, Qingyang Wu, and Yong Jae Lee. Visual instruction tuning. *arXiv preprint arXiv:2304.08485*, 2023.
- Leland McInnes, John Healy, and James Melville. UMAP: Uniform manifold approximation and projection for dimension reduction. *arXiv preprint arXiv:1802.03426*, 2018.
- Sangwoo Mo, Minkyu Kim, Kyungmin Lee, and Jinwoo Shin. S-clip: Semi-supervised vision-language learning using few specialist captions. *Advances in Neural Information Processing Systems*, 36, 2024.
- Michael Moor, Qian Huang, Shirley Wu, Michihiro Yasunaga, Yash Dalmia, Jure Leskovec, Cyril Zakka, Eduardo Pontes Reis, and Pranav Rajpurkar. Med-flamingo: a multimodal medical few-shot learner. In *Machine Learning for Health (ML4H)*, pp. 353–367. PMLR, 2023.
- Norman Mu, Alexander Kirillov, David Wagner, and Saining Xie. Slip: Self-supervision meets language-image pre-training. In *European Conference on Computer Vision*, pp. 529–544. Springer, 2022.
- Muhammad Ferjad Naeem, Yongqin Xian, Xiaohua Zhai, Lukas Hoyer, Luc Van Gool, and Federico Tombari. SILC: Improving vision language pretraining with self-distillation. *arXiv preprint arXiv:2310.13355*, 2023.
- David Nukrai, Ron Mokady, and Amir Globerson. Text-only training for image captioning using noise-injected clip. *arXiv preprint arXiv:2211.00575*, 2022.
- Changdae Oh, Junhyuk So, Hoyoon Byun, YongTaek Lim, Minchul Shin, Jong-June Jeon, and Kyungwoo Song. Geodesic multi-modal mixup for robust fine-tuning. *Advances in Neural Information Processing Systems*, 36, 2023.
- Aaron van den Oord, Yazhe Li, and Oriol Vinyals. Representation learning with contrastive predictive coding. *arXiv preprint arXiv:1807.03748*, 2018.
- Anil Palepu and Andrew Beam. Tier: Text-image entropy regularization for medical clip-style models. In *Machine Learning for Healthcare Conference*, pp. 548–564. PMLR, 2023.
- Alec Radford, Jong Wook Kim, Chris Hallacy, Aditya Ramesh, Gabriel Goh, Sandhini Agarwal, Girish Sastry, Amanda Askell, Pamela Mishkin, Jack Clark, et al. Learning transferable visual models from natural language supervision. In *International conference on machine learning*, pp. 8748–8763. PMLR, 2021.
- Aditya Ramesh, Mikhail Pavlov, Gabriel Goh, Scott Gray, Chelsea Voss, Alec Radford, Mark Chen, and Ilya Sutskever. Zero-shot text-to-image generation. In *International Conference on Machine Learning*, pp. 8821–8831. PMLR, 2021.
- Nils Reimers and Iryna Gurevych. Sentence-BERT: Sentence embeddings using siamese BERT-networks. In *Proceedings of the 2019 Conference on Empirical Methods in Natural Language Processing and the 9th International Joint Conference on Natural Language Processing (EMNLP-IJCNLP)*, pp. 3982–3992, 2019.
- George Shih, Carol C Wu, Safwan S Halabi, Marc D Kohli, Luciano M Prevedello, Tessa S Cook, Arjun Sharma, Judith K Amorosa, Veronica Arteaga, Maya Galperin-Aizenberg, et al. Augmenting the national institutes of health chest radiograph dataset with expert annotations of possible pneumonia. *Radiology: Artificial Intelligence*, 1(1):e180041, 2019.
- Amanpreet Singh, Ronghang Hu, Vedanuj Goswami, Guillaume Couairon, Wojciech Galuba, Marcus Rohrbach, and Douwe Kiela. Flava: A foundational language and vision alignment model. In *Proceedings of the IEEE/CVF Conference on Computer Vision and Pattern Recognition*, pp. 15638–15650, 2022.
- Akshay Smit, Saahil Jain, Pranav Rajpurkar, Anuj Pareek, Andrew Y Ng, and Matthew Lungren. Combining automatic labelers and expert annotations for accurate radiology report labeling using BERT. In *Proceedings of the 2020 Conference on Empirical Methods in Natural Language Processing (EMNLP)*, pp. 1500–1519, 2020.

-
- Kaitao Song, Xu Tan, Tao Qin, Jianfeng Lu, and Tie-Yan Liu. MPNet: Masked and permuted pre-training for language understanding. *Advances in Neural Information Processing Systems*, 33:16857–16867, 2020.
- Hari Sowrirajan, Jingbo Yang, Andrew Y Ng, and Pranav Rajpurkar. MoCo-CXR: MoCo pretraining improves representation and transferability of chest X-ray models, 2021. URL <https://arxiv.org/abs/2010>.
- Zeyi Sun, Ye Fang, Tong Wu, Pan Zhang, Yuhang Zang, Shu Kong, Yuanjun Xiong, Dahua Lin, and Jiaqi Wang. Alpha-clip: A clip model focusing on wherever you want. *arXiv preprint arXiv:2312.03818*, 2023.
- Michael Tschannen, Basil Mustafa, and Neil Houlsby. CLIPPO: Image-and-language understanding from pixels only. In *Proceedings of the IEEE/CVF Conference on Computer Vision and Pattern Recognition*, pp. 11006–11017, 2023.
- Tao Tu, Shekoofeh Azizi, Danny Driess, Mike Schaekermann, Mohamed Amin, Pi-Chuan Chang, Andrew Carroll, Charles Lau, Ryutaro Tanno, Ira Ktena, et al. Towards generalist biomedical ai. *NEJM AI*, 1(3): AIoa2300138, 2024.
- Tom van Sonsbeek, Xiantong Zhen, Dwarikanath Mahapatra, and Marcel Worring. Probabilistic integration of object level annotations in chest x-ray classification. In *Proceedings of the IEEE/CVF Winter Conference on Applications of Computer Vision*, pp. 3630–3640, 2023.
- Vikas Verma, Alex Lamb, Christopher Beckham, Amir Najafi, Ioannis Mitliagkas, David Lopez-Paz, and Yoshua Bengio. Manifold mixup: Better representations by interpolating hidden states. In *International conference on machine learning*, pp. 6438–6447. PMLR, 2019.
- Vikas Verma, Thang Luong, Kenji Kawaguchi, Hieu Pham, and Quoc Le. Towards domain-agnostic contrastive learning. In *International Conference on Machine Learning*, pp. 10530–10541. PMLR, 2021.
- Bin Wang, Hongyi Pan, Armstrong Aboah, Zheyuan Zhang, Elif Keles, Drew Torigian, Baris Turkbey, Elizabeth Krupinski, Jayaram Udupa, and Ulas Bagci. Gazegnn: A gaze-guided graph neural network for chest x-ray classification. In *Proceedings of the IEEE/CVF Winter Conference on Applications of Computer Vision*, pp. 2194–2203, 2024.
- Feng Wang and Huaping Liu. Understanding the behaviour of contrastive loss. In *Proceedings of the IEEE/CVF conference on computer vision and pattern recognition*, pp. 2495–2504, 2021.
- Tongzhou Wang and Phillip Isola. Understanding contrastive representation learning through alignment and uniformity on the hypersphere. In *International Conference on Machine Learning*, pp. 9929–9939. PMLR, 2020.
- Xiaosong Wang, Yifan Peng, Le Lu, Zhiyong Lu, Mohammadhadi Bagheri, and Ronald M Summers. ChestX-Ray8: Hospital-scale chest x-ray database and benchmarks on weakly-supervised classification and localization of common thorax diseases. In *Proceedings of the IEEE conference on computer vision and pattern recognition*, pp. 2097–2106, 2017.
- Zifeng Wang, Zhenbang Wu, Dinesh Agarwal, and Jimeng Sun. MedCLIP: Contrastive learning from unpaired medical images and text. *arXiv preprint arXiv:2210.10163*, 2022.
- Floris Weers, Vaishaal Shankar, Angelos Katharopoulos, Yinfei Yang, and Tom Gunter. Masked autoencoding does not help natural language supervision at scale. In *Proceedings of the IEEE/CVF Conference on Computer Vision and Pattern Recognition*, pp. 23432–23444, 2023.
- Chaoyi Wu, Xiaoman Zhang, Ya Zhang, Yanfeng Wang, and Weidi Xie. Medklip: Medical knowledge enhanced language-image pre-training. *medRxiv*, pp. 2023–01, 2023.
- Hu Xu, Saining Xie, Xiaoqing Ellen Tan, Po-Yao Huang, Russell Howes, Vasu Sharma, Shang-Wen Li, Gargi Ghosh, Luke Zettlemoyer, and Christoph Feichtenhofer. Demystifying clip data. *arXiv preprint arXiv:2309.16671*, 2023a.

-
- Shawn Xu, Lin Yang, Christopher Kelly, Marcin Sieniek, Timo Kohlberger, Martin Ma, Wei-Hung Weng, Attila Kiraly, Sahar Kazemzadeh, Zakkai Melamed, et al. Elixr: Towards a general purpose x-ray artificial intelligence system through alignment of large language models and radiology vision encoders. *arXiv preprint arXiv:2308.01317*, 2023b.
- Kihyun You, Jawook Gu, Jiyeon Ham, Beomhee Park, Jiho Kim, Eun K Hong, Woonhyuk Baek, and Byungseok Roh. CXR-CLIP: Toward large scale chest X-ray language-image pre-training. In *International Conference on Medical Image Computing and Computer-Assisted Intervention*, pp. 101–111. Springer, 2023.
- Feiyang Yu, Mark Endo, Rayan Krishnan, Ian Pan, Andy Tsai, Eduardo Pontes Reis, Eduardo Kaiser Uruahy Nunes Fonseca, Henrique Min Ho Lee, Zahra Shakeri Hossein Abad, Andrew Y Ng, et al. Evaluating progress in automatic chest x-ray radiology report generation. *Patterns*, 4(9), 2023.
- Jure Zbontar, Li Jing, Ishan Misra, Yann LeCun, and Stéphane Deny. Barlow twins: Self-supervised learning via redundancy reduction. In *International Conference on Machine Learning*, pp. 12310–12320. PMLR, 2021.
- Hongyi Zhang, Moustapha Cisse, Yann N Dauphin, and David Lopez-Paz. mixup: Beyond empirical risk minimization. *arXiv preprint arXiv:1710.09412*, 2017.
- Ke Zhang, Yan Yang, Jun Yu, Hanliang Jiang, Jianping Fan, Qingming Huang, and Weidong Han. Multi-task paired masking with alignment modeling for medical vision-language pre-training. *IEEE Transactions on Multimedia*, 2023a.
- Tianyi Zhang, Varsha Kishore, Felix Wu, Kilian Q Weinberger, and Yoav Artzi. BERTScore: Evaluating text generation with BERT. In *International Conference on Learning Representations*, 2019.
- Yuhao Zhang, Hang Jiang, Yasuhide Miura, Christopher D Manning, and Curtis P Langlotz. Contrastive learning of medical visual representations from paired images and text. In *Machine Learning for Healthcare Conference*, pp. 2–25. PMLR, 2022.
- Yuhui Zhang, Jeff Z HaoChen, Shih-Cheng Huang, Kuan-Chieh Wang, James Zou, and Serena Yeung. Diagnosing and rectifying vision models using language. *arXiv preprint arXiv:2302.04269*, 2023b.
- Yuhui Zhang, Elaine Sui, and Serena Yeung. Connect, Collapse, Corrupt: Learning cross-modal tasks with uni-modal data. In *The Twelfth International Conference on Learning Representations*, 2024.